



Variation of boundary-layer wind spectra with height

Larsén, Xiaoli Guo; Petersen, Erik L.; Larsen, Søren Ejling

Published in:
Quarterly Journal of the Royal Meteorological Society

Link to article, DOI:
[10.1002/qj.3301](https://doi.org/10.1002/qj.3301)

Publication date:
2018

Document Version
Peer reviewed version

[Link back to DTU Orbit](#)

Citation (APA):
Larsén, X. G., Petersen, E. L., & Larsen, S. E. (2018). Variation of boundary-layer wind spectra with height. *Quarterly Journal of the Royal Meteorological Society*, 144(716), 2054-2066. <https://doi.org/10.1002/qj.3301>

General rights

Copyright and moral rights for the publications made accessible in the public portal are retained by the authors and/or other copyright owners and it is a condition of accessing publications that users recognise and abide by the legal requirements associated with these rights.

- Users may download and print one copy of any publication from the public portal for the purpose of private study or research.
- You may not further distribute the material or use it for any profit-making activity or commercial gain
- You may freely distribute the URL identifying the publication in the public portal

If you believe that this document breaches copyright please contact us providing details, and we will remove access to the work immediately and investigate your claim.

Variation of boundary-layer wind spectra with height

Xiaoli Guo Larsén*, Erik L. Petersen and Søren E. Larsen

Wind Energy Department, Technical University of Denmark, Risø-Campus, 4000 Roskilde, Denmark

*Correspondence to: xgal@dtu.dk

This study revisits the height dependence of the wind speed power spectrum from the synoptic scale to the spectral gap. Measurements from cup anemometers and sonics at heights of 15 m to 244 m are used. The measurements are from one land site, one coastal land-based site and three offshore sites in the mid-latitudes. There are two new findings. The first finding addresses the diurnal peak in the power spectrum. Our analysis suggests that there are two sources that contribute to the diurnal peak. One is related to surface-driven processes and another one is related to pressure perturbation from the atmospheric tide. The second finding regards the height dependence of the general spectrum. We describe the dependence through a so-called effective roughness, which is calculated from wind spectra and represents the energy removal at different frequencies, and thus surface conditions in the footprint areas. The generalizable spectral properties of winds presented herein may prove useful for validating numerical models.

Key Words: diurnal cycle; diurnal spectral peak; background spectrum; spectral gap; effective roughness

1. Introduction

The height dependence of wind spectra has been relatively well studied for three dimensional (3D) turbulence, e.g. Kaimal and Finnigan (1994). A similar quantitative description of the height dependence of large scale two dimensional (2D) spectra has yet not been established.

In the spectral analysis of 10-min mean wind measurements over water, Larsén *et al.* (2013) observed the variation of the power spectrum $S(f)$ with height for frequency $f < 10^{-3}$ Hz. The dependence was shown to be slightly more obvious at the Nysted site than at Horns Rev 1 mast 2 (hereinafter M2). Nysted is in the Baltic Sea and has a climatologically stable stratification, while Horns Rev is in the North Sea and exhibits a climatologically unstable stratification. Spectral behavior in the gap region (Larsén *et al.* (2016),

[†]This work is partly supported by New European Wind Atlas Project and partly supported by Danish ForskEL project OffshoreWake

This article has been accepted for publication and undergone full peer review but has not been through the copyediting, typesetting, pagination and proofreading process, which may lead to differences between this version and the Version of Record. Please cite this article as doi: 10.1002/qj.3301

hereinafter L16) for $1 \text{ day}^{-1} < f < 10^{-3} \text{ Hz}$ exhibits the following properties: (1) At Høvsøre (a coastal site on land), the depth of the spectral gap decreases with height. This was interpreted as a result of decreasing 3D turbulence contribution and increasing 2D turbulence contribution as the height increases from 10 m to 100 m. (2) At Høvsøre, the spectral power of wind speed increases with height, most significantly below 60 m. At M2 (i.e. offshore), the change of $S(f)$ with height is small above the lowest measurement height 15 m. (3) At Høvsøre, the diurnal peak of the spectrum is striking at 10 m, becomes weak at 40 m and indistinguishable at higher levels. This was interpreted as an indication for a decreasing effect from the land surface with height. At M2, no diurnal peaks were observed from 15 m and above, indicating the absence of a clear diurnal cycle in a climatological sense. This is consistent with the absence of a diurnal peak in measurements from a number of lightships and small island stations (Troen and Petersen 1989). All of the above studies are based on years of measurements and they can be considered “climatological”. Under special diurnal circulations such as the sea breeze, marine stations can also experience a diurnal variation in wind speed, which manifests itself in the diurnal peak in the spectrum, e.g. Lapworth (2005); Barthelmie *et al.* (1996).

The wind variation at frequency $f_d \equiv 1 \text{ day}^{-1}$ reflects the daily cycle oscillation, representing an organized and harmonic processes of the atmosphere. A good understanding of these processes is necessary for numerical modeling of the diurnal cycles, which is still a challenge directly relevant for wind energy application (Emeis 2014). Climatological diurnal variation of wind speed has been previously studied at land sites for heights of 70 to 100 m (e.g. Oort and Taylor (1969) and Petersen (1975)). Troen and Petersen (1989) explained that the height where the diurnal peak becomes weak is where the first-order effect of the surface heat-flux modulations vanishes. The diurnal wind cycle has been studied in the boundary layer, in the free atmosphere with altitudes from 3 to 20 km (Vinnichenko and Dutton 1969), and in the stratosphere (10 mb) (Carlson and Hastenrath 1970). Wieringa (1989) presented an analysis of the daily cycle of the wind speed up to 200 m from the Cabauw site. He defined a reverse height to address where the amplitude of the daily cycle changes from decreasing with height to increasing with height (their Figure 2). The reverse height was demonstrated to be around 80 m with measurements from Cabauw, 90 m from measurements up to 440 m in Oklahoma (Crawford and Hudson 1973), and about 70 m at Nauen in Germany (Hellmann 1917). Wieringa (1989) suggested that in the famous Van der Hoven spectrum for the 100 m wind speed, the absence of the diurnal peak could be caused by the location of the reverse height at this height. Wieringa (1989) observed also that at Cabauw the amplitude of the diurnal cycle is still increasing at 200 m, Byzova (1967) found such an increase up to 300 m and Crawford and Hudson (1973) showed that it is increasing at least up to 440 m. Vinnichenko and Dutton (1969) discovered that the wind spectrum in the free atmosphere is characterized by (1) A diurnal peak that is stronger than close to the earth surface; (2) more energy in the mesoscale range where the time scale is longer than a couple of days, which is speculated to be associated with internal gravity waves, as supported by the analysis in section 5.3 in Larsén *et al.* (2013). From soundings, Carlson and Hastenrath (1970) suggested that the diurnal variation of wind throughout the troposphere is roughly consistent with a pressure perturbation that travels around the globe with the Sun. Atmospheric movement related to this perturbation is sometimes referred to as the atmospheric tide and it yields an amplitude of the surface diurnal wind cycle slightly less than 1 ms^{-1} , as a net effect from modifications from terrains and various types of diffusion processes up to the altitude of 30 km.

The current paper uses meteorological measurements from five stations (Fig. 1), which extend from surface to about 240 m, to examine the variation of the boundary-layer wind spectrum with height, addressing different frequency ranges from synoptic scale to the spectral gap. These measurements are also used to study the spatial structure behind the diurnal variations.

For better readability, some of the key variables and their definitions are listed in Table 1.

The measurements are introduced in section 2 and the method is described in section 3. Results are presented in section 4, followed by discussions and conclusions in section 5.

Table 1. Variables and definitions.

Variable	Definition
f	frequency, Hz
f_p	peak frequency of the 3D turbulence spectrum, Hz
f_h	$f = 1 \text{ h}^{-1}$, Hz
f_d	$f = 1 \text{ day}^{-1}$, Hz
$S(f)$	power spectrum as a function of f , m^2s^{-1}
$S(f_h)$	power spectrum at $f = f_h$, m^2s^{-1}
$S(f_d)$	power spectrum at $f = f_d$, m^2s^{-1}
$S_{reg}(f, z)$	spectral energy given by the linear regression line, as a function of f and z , shown in Fig. 4, m^2s^{-1}
$S_{reg}(f)$	spectral energy given by the linear regression line at a given z , as a function of f , m^2s^{-1}
$S_{reg}(f_d)$	spectral energy as shown by the linear regression line at $f = f_d$, shown in Fig. 4b, m^2s^{-1}
S_p	peak spectral intensity at f_d , shown in Fig. 4b, m^2s^{-1}
$\langle S(f) \rangle$	average of S at f from a collection of power spectra
$\sigma(S(f))$	standard deviation of S at f from a collection of power spectra
z	height, m
z_0	aerodynamic roughness length, m
z_e	effective roughness, m, obtained from Eq. 2 for a given f
a and b	linear regression coefficients in $\ln S(f) = a \ln f + b$, shown in Fig. 4
A and B	linear regression coefficients in Eq. 2, examples shown in Fig. 13

Table 2. Wind speed data at the five sites shown in Fig. 1, the data period, average data coverage for cup anemometer data, measurement height range and the heights where sonic data are analyzed. “-” means no sonic data analyzed.

Site	Period Year/Month	Data Coverage	Cup heights (m)	Sonic heights (m)
Østerild	2015/5 - 2016/5	99.3%	10, 40, 70, 106, 140, 178, 210, 244	7, 37, 103, 175, 241
Høvsøre	2012/1 - 2013/12	98.2%	10, 20, 40, 60, 80, 100, 116.5	10, 20, 80, 100
Høvsøre	2006/1 - 2017/12	97.8%	10, 20, 40, 60, 80, 100, 116.5	-
Horns Rev I M2	2000/1 - 2002/12	99.9%	15, 30, 45, 62	50
Horns Rev II M8	2012/1 - 2013/12	98.0%	27, 37, 47, 67, 77, 87, 97, 107	-
FINO 3	2010/1 - 2013/12	94.9%	30, 50, 100, 106	-

2. Measurements

The measurements include three offshore sites (M2, Horns Rev II M8 (hereinafter M8) and FINO 3) and two land-based sites (Høvsøre and Østerild), see their locations in Fig. 1. From each site, we choose the years when the data coverage is 95% or more, in order to obtain reliable long-term wind spectra. The data length from those sites varies from one year to four years, see Table 2. Details about Høvsøre and M2 can be found in L16 and details about the FINO 3 site can be found in Peña *et al.* (2015). At M8, wind speeds are measured at a meteorological mast from 27 to 107 m. Table 2 lists the data period, average data coverage, and the heights from which cup anemometer and sonic data (if available) from each site are analyzed.

The Østerild southern mast (mast-S) provides us the new record height of 241 m, with mean as well as turbulence measurements. This is a chance to continue the study in L16 and extend our understanding of the height dependence of the spectral behavior at various frequencies, including the diurnal peak and the gap region. Mast-S is surrounded by a variety of topographic features as can be seen in Fig. 2a. To the far north and far west, it is the North Sea and to the south it is a shallow fjord (Limfjorden), and closeby there are forests with tree height of about 30 m. Mast-S, together with another mast in the north (where the measurement period was too short for the analysis), are shown in Fig. 2b in the elevation map.

3. Method

Power spectra have been calculated from the 10-min cup anemometer measurements from the five sites, as well from the 20 Hz sonic measurements from Østerild.

The spectrum is calculated using Fast Fourier Transform after applying linear detrending to the time series. Afterwards, a smoother spectrum is obtained by averaging the spectral power in the bins of $\log_{10} f$, i.e. using log-smoothing.

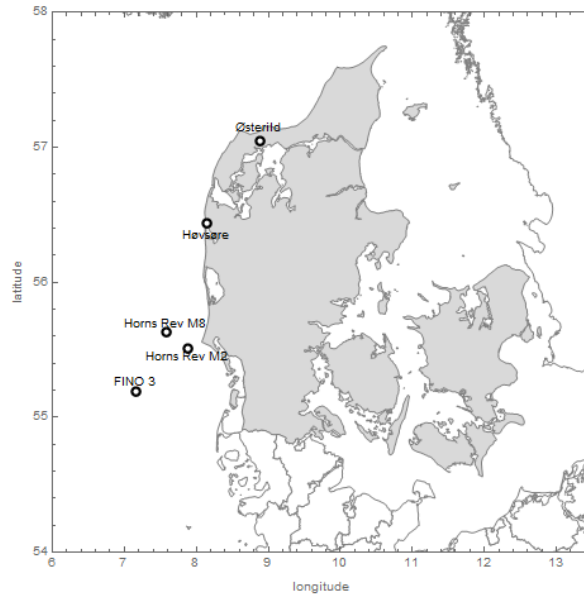


Figure 1. Map of Denmark and the locations of the five sites, Østerild, Høvsøre, Horns Rev I M2, Horns Rev II M8 and FINO 3.

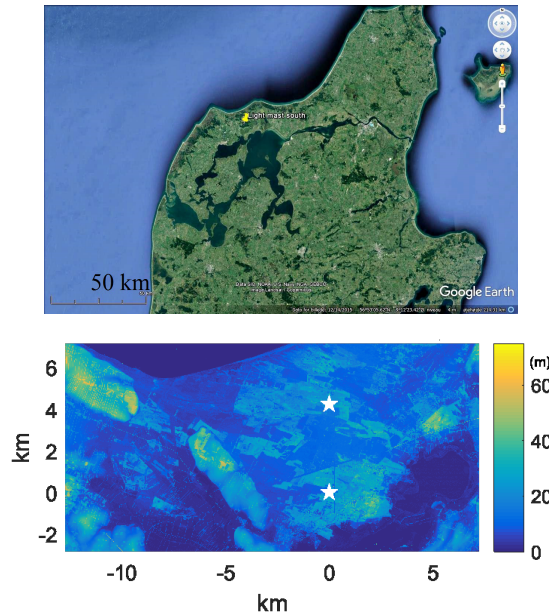


Figure 2. Above: Google map of surroundings of Østerild light-mast-S (highlighted with the yellow mark); Below: Terrain and tree heights of nearby surroundings of the two Østerild light masts, note we only used measurements from the southern mast (prepared by Ebba Dellwik).

For the 10-min mean time series, the few missing data in the time series is first filled in with linear interpolation of data before and after the gaps, before the linear detrending is applied. The log-smoothing is applied using 35 bins for each decade. The number 35 is used here, because of our focus on the diurnal peak ($f_d \equiv 1 \text{ day}^{-1}$). The value of the spectral power at f_d , $S(f_d)$, varies slightly with the number of bins that are used for each decade (for numbers between 25 to 90). When using 35 bins in one decade, the averaged value of the frequencies around 1 day^{-1} is closest to the exact 1 day^{-1} .

In order to examine the spectrum in the gap region up to 241 m height, sonic measurements from Østerild are used to calculate both the 2D (using 10-min mean values) and 3D (using 20 Hz data) wind spectra. The 3D spectra have been calculated in the same manner as in L16 for Høvsøre and M2. The spectrum is first calculated using time series from each day and averaged afterwards to obtain the mean spectrum. For the data from 2015 to 2016, only days where less than 0.05% of the sonic data are missing are included. As discussed in L16, the incomplete turbulence data coverage and uneven data distribution throughout the year may undermine the climatological representativeness of some results from these data. However, L16 showed that such a dataset is sufficient

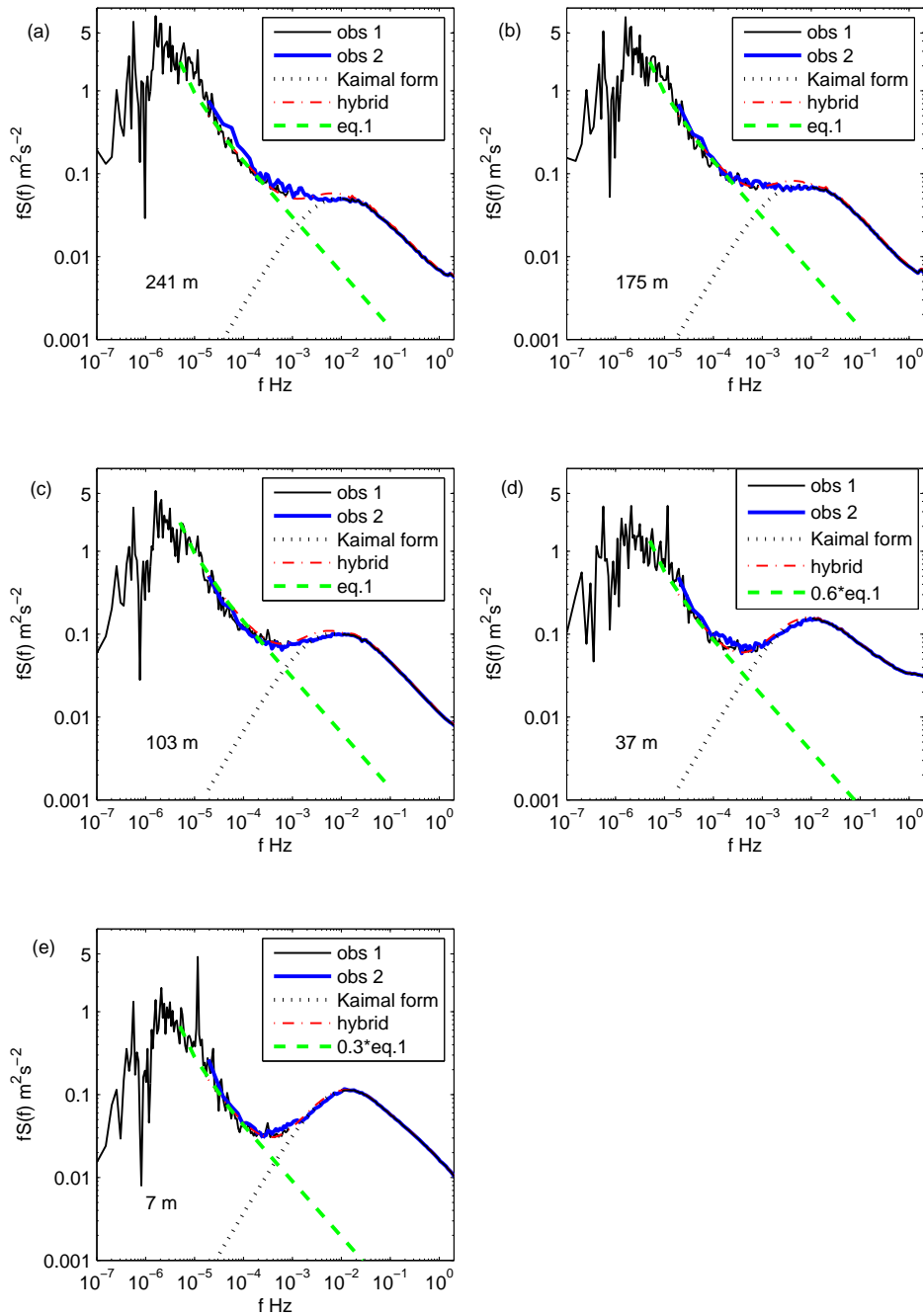


Figure 3. The merge of the spectra of 10-min and 20 Hz sonic wind speeds at five levels at Østerild mast-S. obs 1: 10-min mean wind from sonic; obs 2: average of the 1-day long 20 Hz wind from sonic; Kaimal form: the Kaimal turbulence expression for $f \leq f_p$ which is basically $S(f) = S(f_p)$; hybrid: sum of the green curve and the black dots.

for the analysis of the spectral gap at Høvsøre. In L16, it was discussed that in order to control the possible spectral energy leakage associated with strongly non-stationary conditions, “outliers” were excluded in the calculation of the mean spectrum through requiring $\langle S(f) \rangle - i \cdot \sigma(S(f)) < S(f) < \langle S(f) \rangle + i \cdot \sigma(S(f))$ at each frequency, where $\langle S(f) \rangle$ and $\sigma(S(f))$ are the mean value and standard deviation of S at f ; $i = 2$ was used. For the current dataset at Østerild, to merge the 2D and 3D sonic spectra (Fig. 3), we applied $i = 1$, which removed about 2 to 3% of data at heights of 103 m and above, 10% at 37 m and 11% at 7 m. The difference in using $i = 1$ here for Østerild instead of $i = 2$ as for Høvsøre data may cause the climatological representativeness of the day-long sonic data for the two sites to differ. It also implies that we may need to improve the method to ensure it is equivalent to an analysis of a complete full-year of data. This is however beyond the scope of the current paper. Assuming that the same data with these two different temporal resolutions should provide comparable levels of spectral energy for $f < 10^{-3}$ Hz, we conduct the analysis for Østerild using $i = 1$, so that the 2D and 3D statistics match each other (see section 4.1).

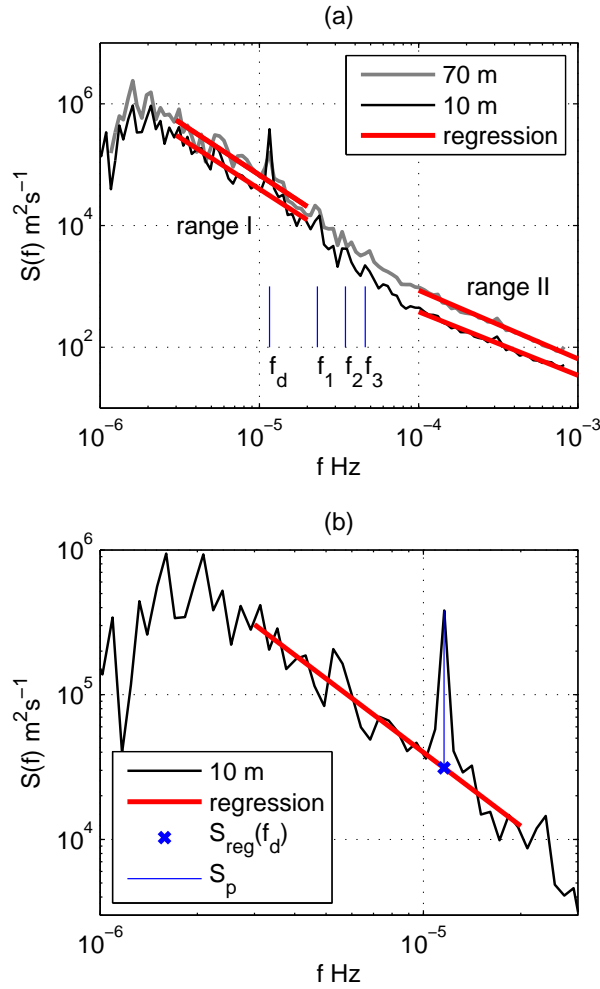


Figure 4. An example of applying the linear regression to the spectra $S(f)$ vs f in log-log coordinates at Østerild for range I and II. (a) Wind speed spectra at 10 m and 70 m, together with the regression lines for range I and II, respectively, using $\ln S(f) = a \ln f + b$. Frequencies of 1 day^{-1} , 12 h^{-1} , 8 h^{-1} and 6 h^{-1} are marked with f_d , f_1 , f_2 and f_3 . (b) below: A close-up of the 10 m spectrum around f_d , where the value on the red regression line, $S_{reg}(f_d)$, is marked with “x” and the peak intensity is marked with a blue vertical line.

In L16, a spectral model was proposed for the gap region. This model is a simple superposition of 3D turbulence for $f < f_p$ (with f_p the 3D spectral peak frequency) and a 2D spectrum model. It was shown in L16 that this simple model reproduces the measured energy in the spectral gap. The 3D turbulence is described by measured spectral energy at f_p which levels off for $f < f_p$, as in the Kaimal model (Kaimal and Finnigan 1994). The 2D spectrum takes the form of

$$S(f) = a_1 f^{-5/3} + a_2 f^{-3}, \quad (1)$$

which was derived in Larsén *et al.* (2013) for the frequency range from approximately 10^{-6} to 10^{-3} Hz. The two coefficients a_1 and a_2 have been obtained from fitting to measurements from a number of stations and they are $a_1 = 3 \times 10^{-4} \text{ m}^2\text{s}^{-8/3}$ and $a_2 = 3 \times 10^{-11} \text{ m}^2\text{s}^{-4}$. In the current study, in order to minimize the fluctuation in the exact values of $S(f)$ as caused by the number of bins for log-smoothing, we apply linear regression to the distribution of $\ln S(f)$ with $\ln f$, and use the values on the regression line (denoted as $S_{reg}(f, z)$ as a function of both f and height z) for this purpose.

To obtain $S_{reg}(f, z)$, we choose narrow frequency ranges so that linear regressions can be applied to obtain a representative value of S at a given f . This avoids the relatively high uncertainty related to obtaining both a_1 and a_2 at the same time through a non-linear regression using Eq. 1. Fig. 4a shows an example of the linear regression in two frequency ranges to the wind spectra from Østerild at 10 m and 70 m, respectively. Range I is $3 \cdot 10^{-6} < f < 2 \cdot 10^{-5}$ Hz and range II is $10^{-4} < f < 10^{-3}$ Hz. The linear regression

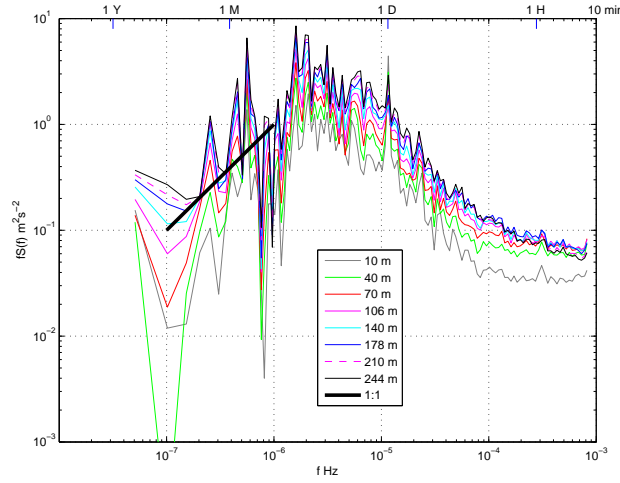


Figure 5. The one-year spectra of cup wind speeds at 8 levels at Østerild mast-S. The scale of 1 year, 1 month, 1 day, 1 hour and 10 minutes are marked on the top of the frame.

thus reads $\ln S(f) = a \ln f + b$. For range I, the pair of data $(f_d, f_d S(f_d))$ is removed when making the regression. For range I, for each site, the estimates of the slope coefficient a at all heights are close to each other. Specifically, at Østerild, the mean of a is -1.73 with a standard deviation of 0.02 from the different heights, i.e., $a = -1.73 \pm 0.02$. Similarly, at Høvsøre, $a = -1.77 \pm 0.008$; at M2, $a = -1.76 \pm 0.03$; at M8, $a = -1.79 \pm 0.02$; at FINO 3, $a = -1.93 \pm 0.02$. Except for FINO3, the overall estimate of a is rather close to $-5/3$, suggesting the dominance of $a_1 f^{-5/3}$ in Eq. 1. The estimate at FINO 3 suggests slightly more influence from $a_2 f^{-3}$. For range II, it is observed that the regression slopes are less steep and the slope varies with height. The flatter slope in range II has also been observed at Høvsøre particularly for the 10 m measurements, which as discussed in L16 (see their Figs 3 and 4) appears to be related to the significant contribution from the 3D turbulence. It will be shown in section 4 that Østerild is more of a land influenced site and the turbulence contribution from the surface is on average more obvious than at Høvsøre.

In relation to the study of height dependence, from the regression lines in range I and II, we extract $S(f)$ at particular frequencies 1 day^{-1} , $(12 \text{ h})^{-1}$, $(8 \text{ h})^{-1}$, $(6 \text{ h})^{-1}$, 1 h^{-1} and $(10 \text{ min})^{-1}$, where the first four frequencies are relevant for the diurnal cycle and the last two are in the spectral gap range.

4. Results

4.1. The full-scale spectra

Following L16, the full-scale wind speed spectra from Østerild are presented in Fig. 3 as $fS(f)$ versus f , where each subplot is for one height. The black curves are calculated from 10-min 1-year sonic measurements and the blue curves are the mean spectra of the 1-day long 20 Hz sonic data. Note that we do not intent to model the 3D turbulence in Fig. 3, where the black dotted curves use the Kaimal model shape for $f \leq f_p$, which basically is a constant $S(f) = S(f_p)$ for $f < f_p$. When addressing $f > f_p$, the measured spectra are used. The peak frequency f_p is identified manually as $\sim 0.01 \text{ Hz}$ where the local maximum $fS(f)$ is located. The green curves in Fig. 3a, b and c, i.e. above 103 m, are the spectral model for the mesoscale range, Eq. 1, extended to higher frequencies. The energy level at lower elevations, 37 m and 10 m, is lower. A regression constrained by Eq. 1 suggests a coefficient 0.6 for 37 m and 0.3 for 10 m to be multiplied to Eq. 1, respectively, to match the energy level for range I. The adjusted mesoscale models are shown as the green curves in Figs. 3d and e. The blended spectral gap model, the sum of the green curve and black dotted curve gives the red dashed curve, from L16 is consistent with measurements up to 241 m. Consistent with L16, the spectral gap is deepest at the surface layer, becomes shallower with height, and here it becomes invisible at 103 m and above.

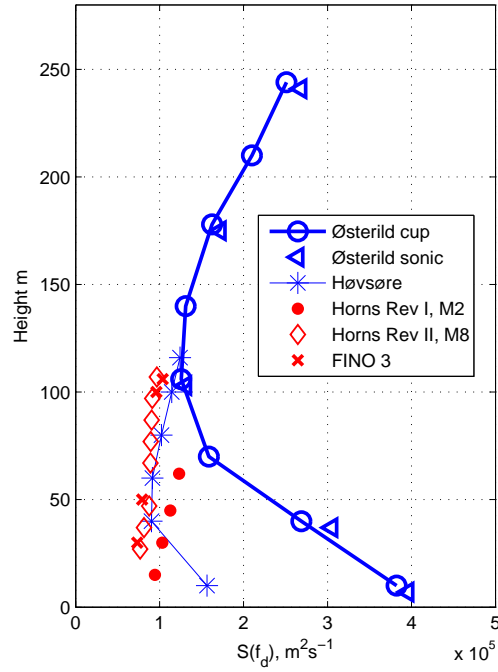


Figure 6. The variation of $S(f)$ with height with $f = f_d$ at the five sites. Blue symbols are group I (offshore sites) and red symbols are group II (land-based) data.

The spectra from the 10-min mean wind speed time series from 10 m to 244 m from mast-S are plotted together in Fig. 5. Comparison with the climatological spectra from Høvsøre in L16 (their Figs. 3, 4 and 6a) indicates the following similarities: (1) For $f < 10^{-6}$ Hz, the spectra $fS(f)$ generally increase with f , following approximately a slope of 1 : 1 in the log-log coordinates. This suggests that the 1-year time series can be considered stationary for spectral analysis; (2) There is a maximum spectral power at $f \approx 2.3 \cdot 10^{-6}$ Hz (approximately 5 days), related to synoptic weather processes; (3) In general the mesoscale power spectrum increases with height. However, Fig. 5 also differs from the Høvsøre spectra. Here the striking peak at $f_d = 1 \text{ day}^{-1}$ is present at all levels from 7 m to 241 m. At Høvsøre the diurnal peak is most clear at 10 m, is weak at 40 m and almost indistinguishable at 80 m.

4.2. Daily cycles

To focus on the diurnal peak, in Fig. 6, we plot $S(f_d)$ at all heights for the five sites. Two groups can be identified from this plot, with group I (red symbols) containing the three offshore sites and group II (blue symbols) the land-based sites. Group I is characterized by a monotonic increase of $S(f_d)$ with height, up to the highest measurement level of 107 m at M8. Group II is characterized by a decreasing of $S(f_d)$ with height first, followed by a reverse and an increase of it with height, consistent with previous observations (see Introduction). At Høvsøre, this reverse occurs at a height of about 40 m and at Østerild, it occurs at about 100 m. Applying the theory from Troen and Petersen (1989), this suggests that the first-order effect of the surface flux modification vanishes at Høvsøre about 40 m, Østerild about 100 m, M2 below 15 m, M8 and FINO 3 below 30 m. Note that for Østerild both the values from the cup and sonic data are presented, and the two show a very good agreement.

Comparing the variation of $S(f_d)$ with height for group I and II in Fig. 6, one can see that, above the reverse height, for group II, $S(f_d)$ increases in a similar manner with height as group I. Could it be that, below this particular height, $S(f_d)$ is dominated by surface processes and above this height, $S(f_d)$ is dominated by another process that is shared by all five sites? To examine this question, we analyze $S(f_d)$ from the most land-influenced site Østerild, and decompose $S(f_d)$ into two parts: S_p and $S_{reg}(f_d)$. Referring to Fig. 4b for the decomposition, here S_p is the diurnal peak intensity (the vertical line) and $S_{reg}(f_d)$ is the value on the red regression line at $f = 1 \text{ day}^{-1}$ (cross). Thus, for data from Østerild, the observed $S(f_d)$ for the eight levels, shown in Fig. 7 as crosses, is decomposed

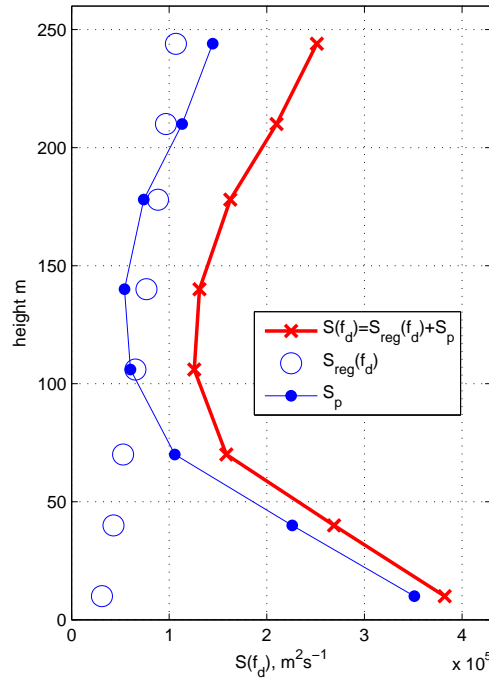


Figure 7. The variation of the power spectra with height at Østerild at $f = 1 \text{ day}^{-1}$, where S is decomposed into the background spectral value without the peak value $S_{reg}(f_d)$ and the magnitude of the peak S_p , so that $S = S_{reg}(f_d) + S_p$.

into $S_{reg}(f_d)$ (circles) and S_p (dots). Below 100 m, $S_p > S_{reg}(f_d)$, with $S_{reg}(f_d)$ moderately increases with height and S_p decreases rapidly with height. S_p becomes smaller than $S_{reg}(f_d)$ at about 100 m, continues decreasing with height until around 140 m and starts to increase, although slightly, with height, and exceeds $S_{reg}(f_d)$ again at about 200 m. The relative contribution from S_p to $S(f_d)$ at 10 m is 92%, decreases to 41% at 140 m and again increases to 57% at 244 m. The increase of $S(f_d)$ above the reverse height appears to be contributed by an increase of both S_{reg} and S_p . The physics behind the increase of S_{reg} is discussed in section 4.3. The cause of the increase of the diurnal spectral peak S_p with height is, as discussed in Introduction, the hypothesized atmospheric tide that results from the periodic heating by the Sun; see detailed discussion in section 5.

The same decomposition is applied to the Høvsøre data, but not to the offshore sites due to the absence of the diurnal peaks at these sites, so for them, $S_{reg}(f_d) = S(f_d)$. $S_{reg}(f_d)$ from the five sites all show a continuous increase with height (Fig. 8). Notably, $S_{reg}(f_d)$ from the offshore sites are close to each other, and they share similar vertical distribution with a rather gentle increase with height. The values of $S_{reg}(f_d)$ are similar for the coastal site Høvsøre (above 10 m) and the offshore sites, and they are larger than those from Østerild. The frequencies $f_1 = (12 \text{ h})^{-1}$, $f_2 = (8 \text{ h})^{-1}$ and $f_3 = (6 \text{ h})^{-1}$ are all relevant for the diurnal cycles. Spectral peaks at these frequencies can be seen in Fig. 4a. However, these peaks are rather weak and the corresponding spectral values are much smaller than S_{reg} , resulting in a monotonic increase of $S(f)$ with height, in contrast to that for $f = f_d$.

We use a second approach to study the diurnal wind variation in the horizontal as well as vertical planet. We calculate the mean wind speed at each hour of the day from the entire time series, see Fig. 9 for the results at the five sites. It can be observed that: (1) The diurnal cycle is more pronounced close to the surface at Østerild and Høvsøre; (2) There is a phase shift of the diurnal cycle of wind speed with height at Østerild and Høvsøre. The shift is most obvious at 140 m at Østerild and 40 m at Høvsøre, and is consistent with the reverse height, and commonly interpreted as resulting from the diurnal cycling of atmospheric stability; (3) At Østerild, the diurnal cycle becomes deeper, again from 140 m; (4) For all three offshore sites, the diurnal variation of wind speed are similar to each other as well as to levels above the reverse height at Østerild and Høvsøre. At the offshore sites the surface driven cycle as present at Østerild and Høvsøre is absent in the measurements.

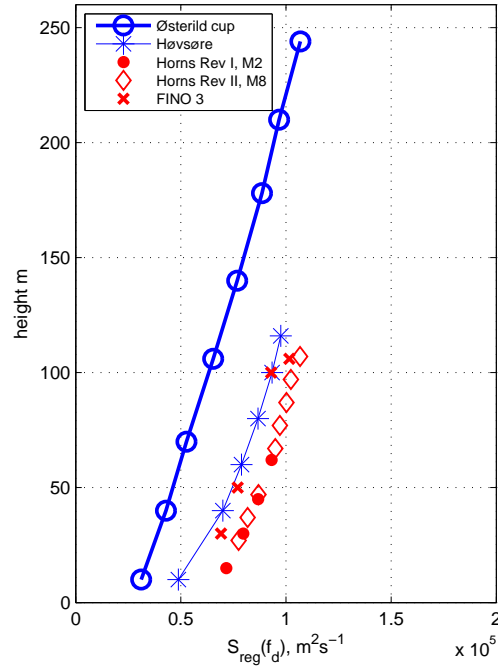


Figure 8. The variation of $S_{reg}(f_d)$ (S with the diurnal peak removed) with height at $f = 1 \text{ day}^{-1}$ at the five sites. As in Fig. 6, blue symbols are group I and red symbols are group II data.

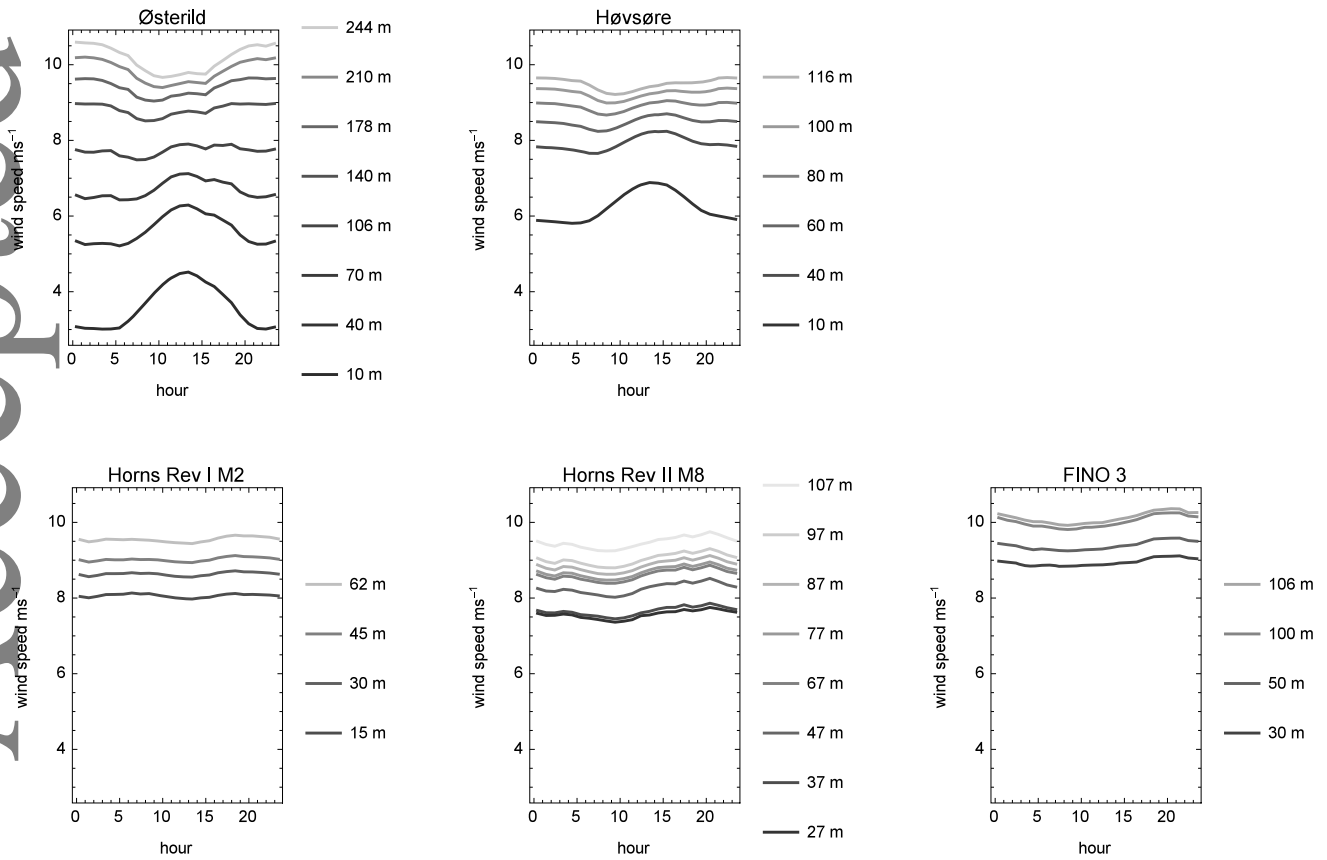


Figure 9. The daily cycle of hourly mean wind speed at several measurement levels at the five sites.

Note that the above analysis is “climatological”, meaning that at a site, all seasons and all conditions are included. At a coastal site like Høvsøre, at 10 m, the analysis suggests that it is an overall land effect that has caused the clear diurnal variation in the hourly mean wind speed (Fig. 9) and the sharp spectral peak at the frequency of 1 day^{-1} . This can be supported by the following analysis. The

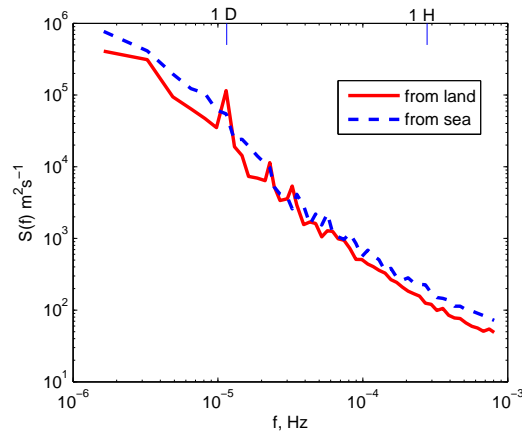


Figure 10. From Høvsøre, the averaged spectra of 10-m wind speed of land segments (with wind from land) and sea segments (with wind from sea) of the entire time series that are longer than 1 week, when the winds are persistently from land or from sea, respectively.

longest time series from the five site, twelve years of 10-m wind speed from Høvsøre, is used to conditionally sample periods with data length longer than one week when winds are persistently from the sea (with direction from 200° to 340° , “sea-segment”) or persistently from land (with direction from 15° to 170° , “land-segment”). A spectral calculation to resolve the signal at a frequency of 1 day^{-1} requires data of tens of, or more, continuous days, and is not possible with the current data set. Using one week-long time series implies relatively high uncertainty of the absolute spectral values at f_d , compared to the use of years of data. Using the above criteria there are 25 land segments and 13 sea segments. The longest segment lasted 18 days. The 25 individual land segment spectra are averaged and shown in Fig. 10 as the red curve. The 13 sea segment spectra are also averaged and shown in Fig. 10 as the blue dashed curve. Note that these segments are only very small portion of the 12 years of data. During some of the land segments, the synoptic weather system obscured the standard diurnal variation (e.g. segment 2010-01-05 to 2010-01-18). From the sea segment, during a sea breeze circulation a diurnal signal may be present (e.g. segment 2012-05-29 to 2012-06-06). In this studied area, winter seasons favor storms, and spring and summer seasons favor sea breezes. In spite of these special individual situations, Fig. 10 suggests that, on average, the spectral peak at f_p is present when winds are from land and it is absent when the winds are from the sea. In Barthelmie *et al.* (1996), in the analysis of summer data from an offshore site Vindeby, a typical land diurnal cycle in wind speeds from land fetch was found present.

The seasonal dependence of the diurnal variation of wind speed has previously been reported in Petersen *et al.* (1981) based on data from a land-based coastal (Risø) mast, which is also in Denmark, about 500 km east of Høvsøre and not far from Østerild. The spectral analysis shown in Figs. 6, 7 and 8 also exhibit seasonality, particularly for land-based sites. For the five sites, we performed a similar calculation in Fig. 9 for each month. Two examples of results are shown in Figs. 11 and 12, with one for land-based site (Høvsøre) and one for offshore site (M8). Østerild has similar results to Høvsøre. M2 and FINO 3 have similar results to M8. For Høvsøre (Fig. 11), there is a strong monthly dependence of the amplitude and vertical variation of the phase shift in the wind diurnal cycle. The wind variation amplitude is largest from April to August and very weak in winter months (November to February). The phase change with height is less obvious in May and December, where for May the surface driven cycle (including sea breeze cases) is strongest and present at all measurement levels and for December it is weakest. For the offshore site M8 (Fig. 12), the diurnal variation is weak for all months and the winds throughout the measurement levels are in phase with each other.

4.3. The height dependence in different frequency ranges

Our earlier studies of the wind spectra for meso- and macro-scales found the variation of $S(f)$ with height in measurements from a number of sites (seven sites in Larsén *et al.* (2013) and two in L16). The variation is however small in the mesoscale range (about 1

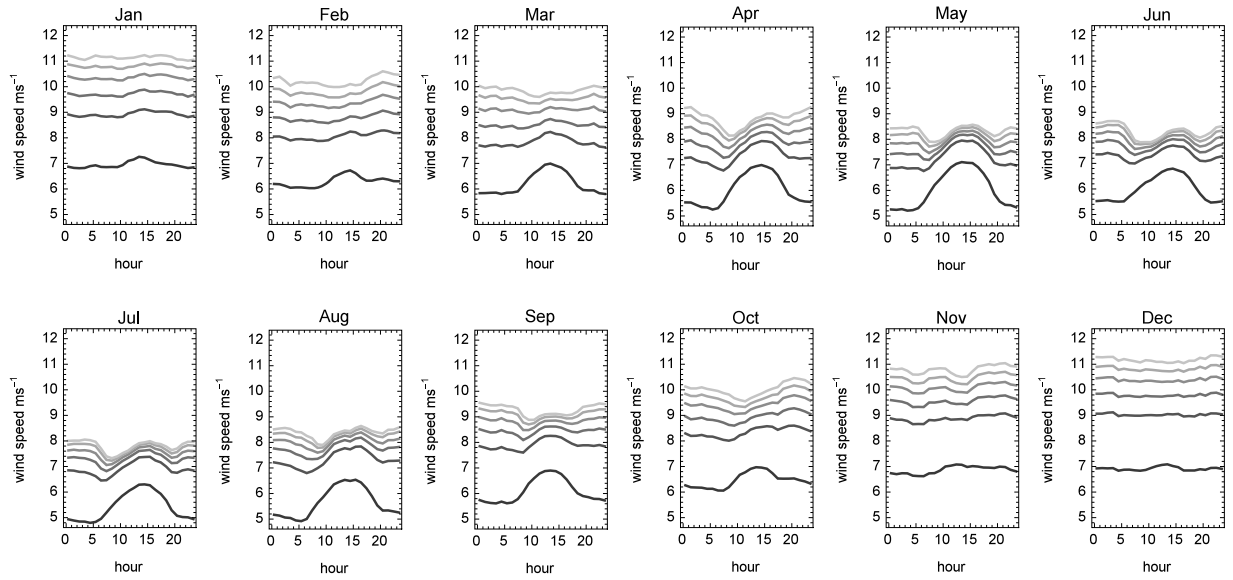


Figure 11. The daily cycles of hourly mean wind speeds at 6 measurement heights at Høvsøre in 12 months. The legend for the curves in each subplot is the same as the plot for Høvsøre in Fig. 9.

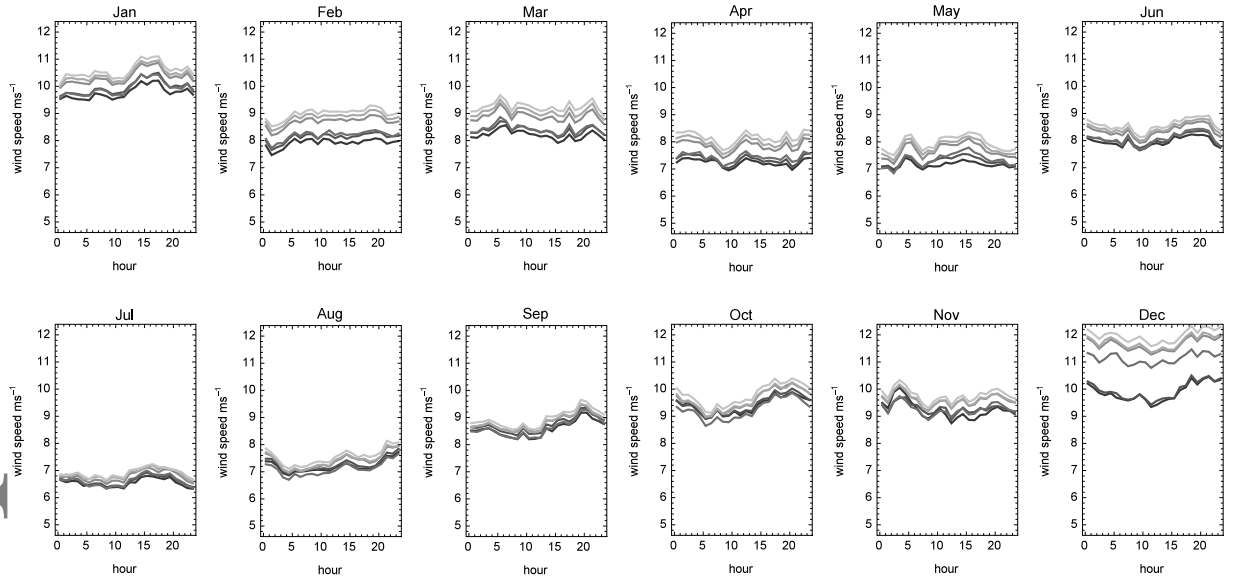


Figure 12. The daily cycles of hourly mean wind speeds at 8 measurement heights at Horns Rev II M8 in 12 months. The legend for the curves in each subplot is the same as the plot for Horns Rev II M8 in Fig. 9.

day⁻¹ to 10⁻³ Hz), and it is speculated to be site-dependent. These studies show that the height variation seems to be different for different frequency ranges and it is more obvious for $f < 1 \text{ day}^{-1}$.

Figure 8 shows consistent height variation of $S_{reg}(f_d)$ across the five sites. Figure 9 shows that the diurnal variation of the mean wind speed at the offshore sites are similar to each other; they are also similar to the land-based sites above the reverse height. This spatial consistency is interpreted here to be related to a common large scale background flow over the region and shared by the five sites. Following the trend of $S_{reg}(f_d)$ varying with height as shown in Fig. 8, these five profiles appear to converge at a height above 110 m. Analogous to a wind speed profile, the difference between these $S_{reg}(f_d)$ -profiles below 110 m could be caused by overall differences of the surface condition between these sites. The background flow corresponding to f_d , with a scale proportional to $U \cdot f_d^{-1}$ with U the mean wind speed representing the upwind fetch, when approaching the surface, interacts with the local terrain which, over their respective upwind fetch of the measurements, may have acted as a kind of drag and therefore momentum sink. Among the five sites, this drag is expected to be largest at Østerild, which is surrounded by forest, land and lakes. Høvsøre is right at the coast, with

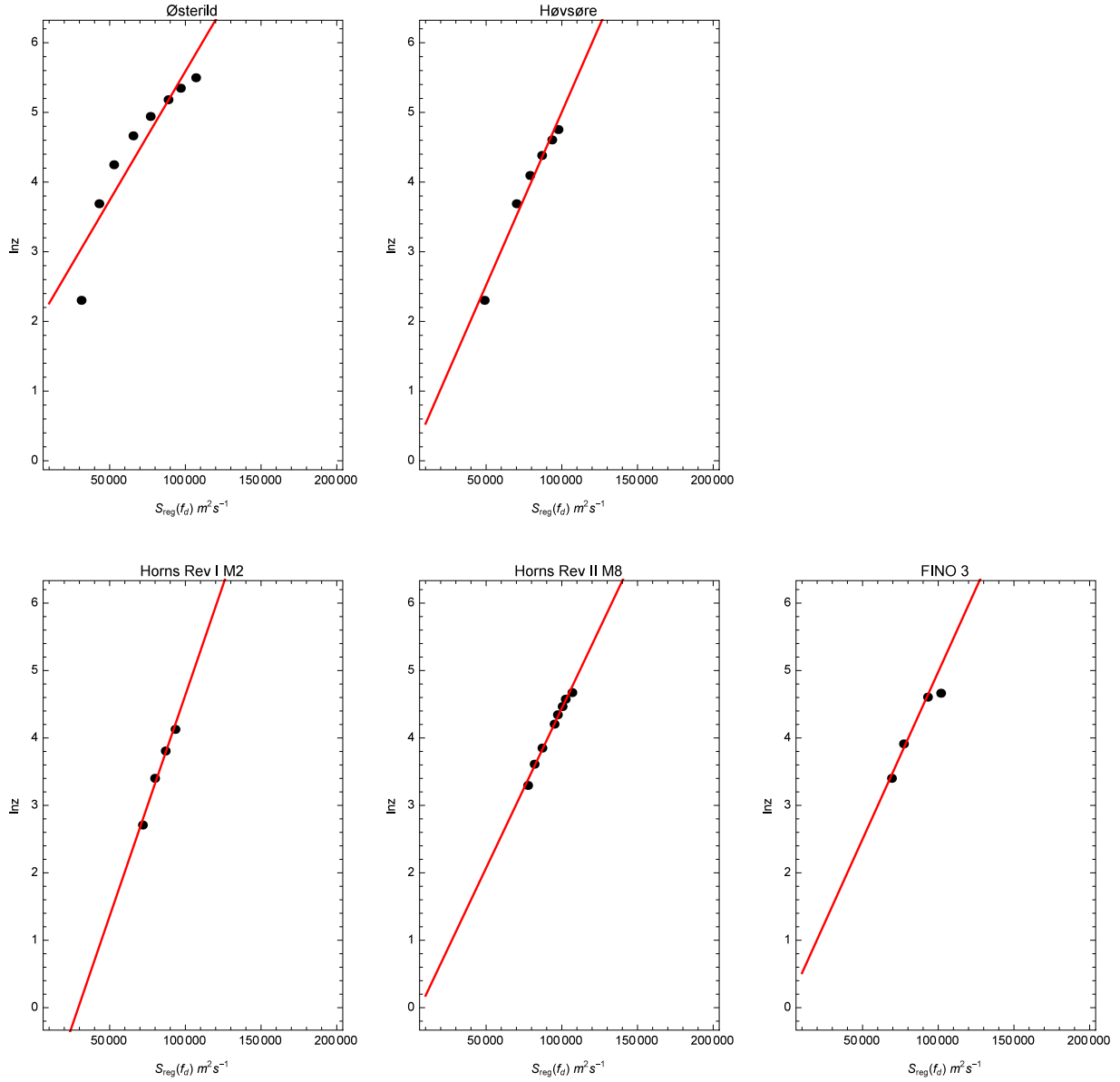


Figure 13. Obtaining z_e by applying Eq. 2 for $f = f_d$ for the five sites, where dots are $S_{reg}(f_d)$ from measurements and the solid lines are Eq. 2.

the winds often from the sea. The offshore sites are smoothest, corresponding to the smallest drag, the smallest momentum sink and therefore the largest $S_{reg}(f_d)$. We here define the effect of the large scale drag with the phrase “effective roughness”, denoted as z_e .

Similar to the estimation of aerodynamic roughness length z_0 from a logarithmic profile of mean wind, we calculate z_e from a vertical logarithmic profile of S_{reg} at a chosen frequency f (see Fig. 13 as an example for $f = f_d$). Although the calculation of z_0 should be done in the atmospheric surface layer, for z_e , we use measurements from all levels to estimate the overall effect. At a chosen f , through:

$$\ln z = AS_{reg} + B, \quad (2)$$

where $S_{reg} = S_{reg}(f, z)$, $z_e(f)$ is obtained as the height where the extrapolation of the profile of S_{reg} with $\ln z$ reaches 0. Thus, $z \rightarrow z_e(f)$ when $S_{reg}(f, z) \rightarrow 0$, so that $z_e(f) = e^B$. A and B are regression coefficients.

It can be derived from Eq. 2 and $\ln S(f) = a \ln f + b$ that, at one particular site, the change of B with f is determined by coefficient a . Calculations in section 3 show that, at one site, for range I, linear regression using $\ln S(f) = a \ln f + b$ gives similar estimate of a at all heights. This in turn will result in similar estimates of z_e at different f in range I. Figure 13 shows results of using Eq. 2 at the five sites. For Østerild, Høvsøre, M2, M8 and FINO 3, the corresponding values of z_e at $f = f_d$ are 6.6 m, 1.0 m, 0.2 m, 0.7 m and 1.0 m,

respectively and the corresponding values of z_e at $f = 0.5 \text{ day}^{-1}$ are similar, as expected, being 6.7 m, 1.1 m, 0.3 m, 0.7 m and 1.4 m, respectively.

For range II, the values of a can vary considerably with height (e.g. Fig. 4a), resulting in different distribution of S_{reg} with $\ln z$ at different f and hence different estimates of z_e at these frequencies. It is known that for the 3D turbulence (normally with frequencies higher than about 10^{-3} Hz), the spectral energy decreases with height as the turbulence is surface driven. The 3D turbulence meets the 2D turbulence in the gap region, determining the height dependence of $S(f)$ there. In Fig. 14, in the gap region, $S_{reg}(f)$ with $f = f_h \equiv 1 \text{ h}^{-1}$, $S_{reg}(f_h)$, is plotted as a function of height z . The energy level is low at f_h compared to lower frequencies. The increase of $S(f_h)$ with height is very small, and is mostly confined to $z < 50 \text{ m}$. Corresponding to flows of the scale of $U \cdot 1 \text{ h}^{-1}$, $z_e(f_h)$ are 1.2 m, 0.11 m, $8 \cdot 10^{-5} \text{ m}$, 0.18 m and 10^{-3} m at Østerild, Høvsøre, M2, M8 and FINO 3, respectively, much smaller than $z_e(f_d)$. The vertical variation of $S_{reg}(f)$ at $f = (10 \text{ min})^{-1}$ is even smaller (not shown).

In the above analysis, we have approximated the flow scale from the upwind fetch as a function of $U \cdot f^{-1}$. To evaluate and refine the above conclusions on how exactly the upwind affect the spectral power distribution, it would be useful to perform spectral analysis for sectors where surface conditions are different. For instance for Østerild, the sectors should be divided for farm land, for forest, for lakes and for sea etc. This classification is relevant for applying a standard and simple footprint model such as Kljun *et al.* (2015). It is impossible here due to the availability of only one-year data from Østerild, which means there are insufficient samples for each sector. Results in Fig. 10 do, however, confirm the conclusion of general effects from land and sea, respectively.

Note that an accurate estimate of the fetch for wind speeds at a certain height is challenging. Kljun *et al.* (2015)'s model would suggest an extent of 80% crosswind-integrated footprint at a peak location of several hundreds of meters at an elevation of 10 m with a roughness length of 0.1 m. With the same roughness length, the main contribution to the signal measured at 100 m is estimated to be located at a distance of several kilometers. The distance is smaller if the roughness length is smaller from an upwind terrain location. The simple model was meant for scalar flux with a known source and homogenous surface condition. The upwind fetch concept we are addressing for the large scale background flow is not consistent with Kljun *et al.* (2015)'s model. According to Kljun's model, the 10-m winds at Høvsøre do not represent the water condition, even when the winds are from the sea. We can therefore only limit our discussion about the footprint, or rather, the upwind fetch for the large scale wind speed in a qualitative manner, e.g. through z_e .

5. Discussion and conclusions

This study revisited the diurnal cycle of wind speed. This is a topic started 100 years ago and it has been studied from the surface layer up to 30 km in the stratosphere. Measurements from meteorological masts, airplanes and radio soundings, over land as well as over water, have been analyzed. Often, the diurnal cycle is studied through the 24-hour variation of the mean wind speed distribution. Observations in the boundary layer have shown that such a diurnal cycle changes phase with height, leading to that the net amplitude first decreases and later increases with height. Causes of this height dependence have not been fully clarified in the literature. Here we use a new approach through a simple spectral decomposition of the power spectrum of year-long wind speed time series, to study the wind variation related to the diurnal cycle. The power spectrum S at $f = f_d \equiv 1 \text{ day}^{-1}$ is decomposed into two parts, one representing the peak intensity (S_p) and one representing a normal wind variation ($S_{reg}(f_d)$), so that $S(f_d) = S_p + S_{reg}(f_d)$. Our analysis suggests that two sources contribute to S_p . The first source is surface-driven, shown as a decreasing power spectrum with height. Such a decrease is more obvious at the most land-condition site Østerild, relatively weak at the coastal site Høvsøre, and absent at the three offshore sites above their lowest measurement level of 15 m. The second source to S_p is characteristic of an increase of S_p with height above the reverse height. We found the concept of the atmospheric tides from the literature (see Introduction) is a suitable interpretation. According to this concept, the periodic heating of the atmosphere by the Sun generates the atmospheric tides and thus a travelling pressure disturbance. The pressure disturbance propagates in the atmosphere where density changes with height significantly and

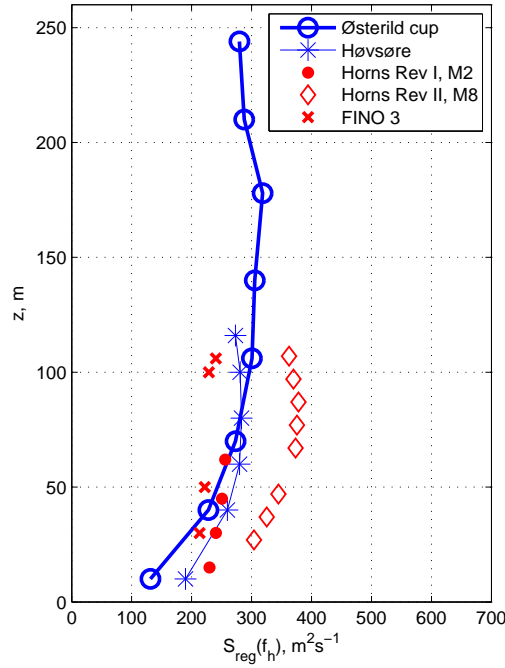


Figure 14. The variation of S at $f = 1 \text{ h}^{-1}$ with height z . As in Fig. 6, blue symbols are group I and red symbols are group II data.

consequently the amplitude of the tides increases with height (Vinnichenko 1970). While the spectral peak intensity S_p below the reverse height reflects more local effects, $S_{reg}(f_d)$ represents more of the larger scale wind variation. Accordingly, $S_{reg}(f_d)$ from the five sites increase with height in a similar manner.

We also analyzed the height dependence of the spectrum for different frequencies from synoptic scale to the spectral gap. To avoid fluctuations in the exact values of S from measurements, linear regression is applied to two frequency ranges (range I: $3 \cdot 10^{-6} < f < 2 \cdot 10^{-5} \text{ Hz}$ and range II: $10^{-4} < f < 10^{-3} \text{ Hz}$), and values from these fits, S_{reg} , are used to study the height dependence. Analogous to the vertical mean wind profile, which is a result of surface roughness and upper air wind forcing such as the geostrophic wind, the vertical profile of S_{reg} at f can be interpreted as a net result of surface drag and the upper air winds under the impact of e.g. the geostrophic wind forcing and gravity waves. The decrease of $S_{reg}(f)$ toward the surface is a representation of the momentum sink. An effective roughness, z_e , is derived to describe this sink. Different from the aerodynamical roughness length z_0 which is obtained from atmospheric surface layer measurements, z_e is calculated for a particular frequency f over the entire measurement level. For measurements up to 100 m, such an estimate may represent a far upwind fetch wind conditions. Specifically, z_e is obtained here by applying a logarithmic dependence of the power spectrum $S_{reg}(f)$ on z at a certain frequency f . At a given site, for range I, the variation of the linear regression slope with height is negligible, resulting in similar estimate of z_e at different f . Such a variation could however be considerable for range II. This is interpreted as a result of 3D turbulence in the gap region (at a time scale of about 10 min to a couple of hours), according to the theories from L16. The relative contribution from the 2D and 3D turbulence changes with height, resulting in a highly uncertain estimate of z_e in the gap region.

With the new measurements at Østerild, we extended and confirmed the gap-region turbulence theory from L16 up to 241 m. In agreement with the findings in L16, the current analysis supports the theory that in the gap region, up to 241 m, the spectrum is a superposition of the weakly or un-correlated 2D and 3D turbulence, and the gap is deeper closer to the surface, becomes shallower with height and invisible eventually.

The findings from the current study are relevant for wind energy applications. Numerical modeling has become a powerful tool in producing time series of wind speed, often with an intention to resolve the diurnal cycles. The method developed here for analyzing the spectral signals may be useful in evaluating numerical modeling results.

The spectral properties are calculated from the entire time series, thus the seasonal impact and thermal stability issues are not addressed specifically.

Acknowledgement

We thank the TEM section from DTU Wind Energy for the data from Østerild, and DONG Energy and Vattenfall for data from Horns Rev I M2 and DONG Energy for data from Horns Rev II M8. We acknowledge MARINET project for the access to the FINO 3 data. The authors thank the New European Wind Atlas project and the Danish ForskEL OffshoreWake project (64017 – 0017/12521) for part of the support. We thank Prof. Sara C. Pryor (Cornell) for the help with language. The authors have no conflicts of interest to declare.

References

- Barthelmie R, Grisogono B, Pryor S. 1996. Observations and simulations of diurnal cycles of near-surface wind speeds over land and sea. *Journal of Geophysical Research* **101**: 21 327–21 337.
- Byzova NL. 1967. *Characteristics of the wind velocity and temperature fluctuations in the atmospheric boundary layer, in Proceeding of the International Colloquium on Atmospheric Turbulence and Radio Wave Propagation. Moscow*. Publishing House Nauka, Moscow.
- Carlson GC, Hastenrath S. 1970. Diurnal variation of wind, pressure and temperature in the troposphere and stratosphere over Eniwetok. *Monthly Weather Review* **98**: 408–416.
- Crawford KC, Hudson HR. 1973. The diurnal wind variation in the lowest 1500 ft in central Oklahoma, June 1966 - May 1967. *J. App. Meteorol.* **12**: 127–132.
- Emeis S. 2014. Current issues in wind energy meteorology. *Meteorological Applications* **21**: 803–819.
- Hellmann G. 1917. Über die bewegung der luft in den unterste schichten der atmosphäre. *Meteorol. Zeitschr* **34**: 273–285.
- Kaimal J, Finnigan J. 1994. *Atmospheric boundary layer flows*. Oxford University Press, New York, 289 pp.
- Kljun N, Calanca P, Rotach M, Schmid H. 2015. A simple two-dimensional parameterisation for Flux Footprint Prediction (FFP). *Geosci. Model Dev.* **8**: 3695–3713.
- Lapworth A. 2005. The diurnal variation of the marine surface wind in an offshore flow. *Q. J. R. Meteorol. Soc.* **131**: 2367–2387.
- Larsén XG, Larsen SE, Petersen EL. 2016. Full-scale spectrum of boundary-layer winds. *Boundary-Layer Meteorol* **159**: 349–371.
- Larsén XG, Vincent CL, Larsen S. 2013. Spectral structure of the mesoscale winds over the water. *Q. J. R. Meteorol. Soc.* **139**: 685–700, doi:DOI: 10.1002/qj.2003.
- Oort AH, Taylor A. 1969. On the kinetic energy spectrum near the ground. *Mon. Weather Rev.* **97**: 623–636.
- Peña A, Gryning S, Floors R. 2015. Lidar observations of marine boundary-layer winds and heights: a preliminary study. *Meteorol. Z.* **24**: 581–589.
- Petersen E. 1975. On the kinetic energy spectrum of the atmospheric motions in the planetary boundary layer. Technical Report RISØ285, Risø National Laboratory, Roskilde, Denmark, http://www.risoe.dk/rispubl/reports_INIS/RISO285.pdf.
- Petersen E, Troen I, Frandsen S, Hedegaard K. 1981. Wind atlas for Denamrk. A rational method for wind energy siting, 229 pages. Technical report, Risø National Laboratory.
- Troen I, Petersen EL. 1989. *European wind atlas*. Risø National Laboratory, Roskilde, Denmark, ISBN 87-550-1482-8, 656 pp, http://orbit.dtu.dk/files/112135732/European_Wind_Atlas.pdf.
- Vinnichenko NK. 1970. The kinetic energy spectrum in the free atmosphere - 1 second to 5 years. *Tellus* **22**: 158–166.
- Vinnichenko NK, Dutton J. 1969. Empirical studies of atmospheric structure and spectra in the free atmosphere. *Radio Sci* **4**: 115–126.
- Wieringa J. 1989. Shapes of annual frequency distributions of wind speed observed on high meteorological masts. *Boundary-Layer Meteorol.* **47**: 85–110.